Pharmaceutical Research, Vol. 23, No. 10, October 2006 (© 2006)
DOI: 10.1007/s11095-006-9052-z

Research Paper

Kinetics and Mechanism for the Reaction of Cysteine with Hydrogen Peroxide in Amorphous Polyvinylpyrrolidone Lyophiles

Dayong Luo[1] and Bradley D. Anderson[1,2]

Received January 29, 2006; accepted May 5, 2006; published online September 2, 2006

Purpose. Peroxide impurities play a critical role in drug oxidation. In metal-free aqueous solutions, hydrogen peroxide (H_2O_2) induced thiol oxidation involves a bimolecular nucleophilic reaction to form a reactive sulfenic acid intermediate (RSOH), which reacts with a second thiol to form a disulfide (RSSR). This study examines the reaction of cysteine (CSH) and H_2O_2 in amorphous polyvinylpyrrolidone (PVP) lyophiles to explore the possible relevance of the solution mechanism to reactivity in an amorphous glass.

Materials and Methods. Amorphous PVP lyophiles containing CSH and H_2O_2 at varying initial 'pH' and reactant concentrations were prepared by methods designed to minimize reaction during lyophilization. Kinetic studies were conducted anaerobically at 25°C and reactants and products were monitored by HPLC. Products were characterized and the kinetic data were fit to models adapted from the solution mechanism.

Results. Key differences in the reactions in aqueous solution and amorphous PVP are: (1) while only cystine (CSSC) forms in solution, three degradants—cysteine sulfinic acid (CSO_2H), cysteine sulfonic acid (CSO_3H) and cystine (CSSC)—form in amorphous PVP; (2) simple bimolecular kinetics govern the solution reaction while initial rates in amorphous PVP suggested more complex kinetics (i.e., non-unity values for reaction order); and (3) heterogeneous (i.e., biphasic) reaction dynamics are evident in amorphous PVP. The differences in product formation and apparent reaction orders in the solid-state could be rationalized by partitioning of the same reactive intermediate to multiple products in the solid-state due to the restricted mobility of CSH. Beyond the initial rate region, the kinetics in amorphous PVP could be described by the Kohlrausch-Williams-Watts (KWW) stretched-exponential equation or by assuming two populations of reactant molecules having different reactivities.

Conclusions. When reactive intermediates are involved, differences in degradant profiles and other characteristics (e.g., rate constants, apparent reaction order) in the amorphous-state may simply reflect altered rates for individual reaction steps due to glass-induced changes in relative reactant mobilities rather than a change in overall mechanism.

KEY WORDS: amorphous solids; chemical kinetics; cysteine; drug stability; hydrogen peroxide; lyophilization; nucleophilic substitution; poly(vinylpyrrolidone); solid-state kinetics; thiol oxidation.

INTRODUCTION

Despite the fact that most commercial drug products are solid dosage forms—particularly tablets, capsules, and lyophilized products—few formal methodologies are currently accepted or widely employed to treat drug degradation kinetics in solid formulations. Moreover, one method which is routinely utilized, the application of the Arrhenius equation to extrapolate accelerated stability data to lower temperatures, may have uncertain reliability for reactions occurring in solids, particularly near a phase transition (1–3). Beyond the Arrhenius model, predictive models for relating solid-state stability to various formulation and storage conditions are seldom applied, making it necessary to produce each formulation being considered and test its stability. In contrast, a comprehensive mathematical and conceptual framework does exist for the analysis of kinetic data for drug degradation in solution formulations, from which it is possible to determine reaction order, characterize reactive intermediates, determine rate constants for various reaction steps and their pH and temperature dependence, and identify the contributions of various ionizable species to the overall reaction rate (4,5).

Amorphous solid pharmaceutical formulations are becoming increasingly important due to a rising interest in amorphous oral formulations with improved bioavailability profiles (6,7) and an increase in the number of peptide, protein, and other biomolecule drug products being formulated in freeze-dried form for reconstitution prior to their use (8–10). The contributions of Zografi and his coworkers (11–17) in particular, have drawn the attention of the pharmaceutical community to the physical characteristics and significance of the amorphous state and the influence

[1] Department of Pharmaceutical Sciences, University of Kentucky, ASTeCC Bldg., Room A323A, Lexington, Kentucky 40506, USA.
[2] To whom correspondence should be addressed. (e-mail: bande2@email.uky.edu)

of residual water on molecular mobility and the solid-state degradation of drugs. Nevertheless, better tools are urgently needed to predict drug stability in amorphous dosage forms.

Bearing in mind Angell's characterization of amorphous glasses as liquids that have lost their ability to flow (18), one might reasonably expect that certain attributes of the solution kinetics of a given drug molecule may carry over to reactions of the same compound occurring in amorphous matrices. Unfortunately, reaction kinetics in amorphous solids are much more complex for a number of reasons. Most importantly, while diffusion-controlled decomposition reactions seldom need to be considered in pharmaceutically relevant solution formulations, molecular mobility plays a critical role in amorphous solid-state reaction kinetics (14,16). Although amorphous glasses are highly viscous, molecular motion is not completely suppressed. As a result, amorphous systems continue to undergo relaxation toward their equilibrium state over time, with corresponding changes in properties (e.g., density) that may affect chemical reactivity. Spatial heterogeneity in these dynamic relaxation processes (19,20) and their time dependence (21,22) as well as possible heterogeneity in the distribution of drug molecules, water, and other formulation components even in amorphous glass excipients such as PVP (2,23,24) may also be important.

While such factors undoubtedly complicate reaction kinetics and may result in changes in both rate-determining steps and preferred reaction pathways for a given compound, some knowledge acquired in solution studies may be transferable to amorphous systems. In this study, we explored the reaction of cysteine (CSH) and H_2O_2 as a function of their concentrations in amorphous polyvinylpyrrolidone (PVP) lyophiles prepared at a fixed 'pH' in order to ascertain the extent to which an understanding of the reaction mechanism in aqueous solution might provide guidance in rationalizing the reaction kinetics and product formed in an amorphous glass. Previously we and others have demonstrated (25–28) that, in the absence of metal ions, thiol oxidation by hydrogen peroxide (H_2O_2) in aqueous solutions involves a two-step bimolecular nucleophilic substitution mechanism, in which the rate-determining formation of a reactive sulfenic acid intermediate (RSOH) is followed by reaction with a second thiolate to form a disulfide (RSSR), the only product observed in aqueous solutions except at extremely high ratios of H_2O_2:RSH.

The amorphous solid-state reaction produces multiple degradation products and exhibits a decidedly more complex rate law governing the reaction (which was shown to be first order with respect to each reactant in solution). In this paper we characterize these differences and explore the hypothesis that such dramatic differences between the solid-state and solution reactions can be rationalized by invoking the same reaction mechanism (i.e., involving the formation of the same sulfenic acid intermediate) once molecular mobility considerations are taken into account.

MATERIALS AND METHODS

Reagents

Cysteine (>98% purity by TLC), cystine (SigmaUltra, >99% purity by TLC), cysteine sulfinic acid (monohydrate), cysteic acid, and polyvinylpyrrolidone K90 (PVP, M_r ~360,000) were purchased from Sigma Chemical Co. (St. Louis, MO). Sodium phosphate dodecahydrate ($Na_3PO_4{\cdot}12H_2O$) was purchased from Aldrich Chemical Company, Inc. (Milwaukee, WI). Sodium dihydrogen phosphate monohydrate ($NaH_2PO_4{\cdot}H_2O$), dibasic sodium phosphate heptahydrate ($Na_2HPO_4{\cdot}7H_2O$), and H_2O_2 (30% aqueous solution) were obtained from Mallinckrodt Baker Inc. (Phillipsburg, NJ). All reagents were analytical grade and used as supplied. Deionized ultra-filtered (DIUF®) water used to prepare CSH and H_2O_2 solutions and HPLC grade acetonitrile were purchased from Fisher Scientific Co. (Pittsburgh, PA). Water used to prepare mobile phases was deionized and further purified through a Milli-Q® UV Plus Ultra-pure Water System, Millipore Ltd. (Billerica, MA).

Lyophile Preparation and Storage

Lyophiles for kinetic studies were prepared by mixing separate phosphate buffered (50 mM, pH 4.0 or pH 6.0) stock solutions of PVP (100 mg/ml), CSH (10, 20, and 40 mM) and H_2O_2 (10, 20, 40, and 50 mM) with the same buffer to produce final solutions containing 10 mg/ml PVP, 1–8 mM CSH, and 1–8 mM H_2O_2 in 50 mM phosphate buffer. Stock solutions of CSH and H_2O_2 were prepared immediately prior to their use. Then 50 or 100 μl aliquots of the H_2O_2 stock solution were transferred to 2 ml glass vials already containing 50 μl of the PVP stock solution and a pre-calculated amount of 50 mM phosphate buffer necessary to achieve a final volume of 0.5 ml. Finally, 50 or 100 μl aliquots of the CSH stock solution were added, mixed rapidly on a vortex mixer for 5 s, then quick-frozen by immersion of the vial in liquid nitrogen to minimize the extent of reaction prior to lyophilization. The vials were held in the liquid N_2 bath for another 5 min after they were frozen then transferred to a tray freeze dryer (FTS Systems, Inc., Stone Ridge, NY) pre-cooled to a shelf temperature of −45°C. The shelf temperature was maintained at −45°C throughout the drying cycle time of 24 h. Vials were capped before breaking the vacuum and placed in the controlled temperature chamber to begin the kinetic studies.

For DSC and powder X-ray diffraction analyses, larger lyophile batches were prepared from solutions containing 20 mg/ml PVP in 50 mM phosphate buffer (pH 4.0 or 6.0) either with or without 5 mM CSH and 5 mM H_2O_2.

Lyophile Characterization

Water Content

The amount of lyophile in each sample was obtained by subtracting the empty vial weight from the total weight of sample plus vial. Samples ($n = 3$) from each batch of lyophile produced were dissolved by adding 1 ml DMSO and the exact amount of DMSO/lyophile was obtained by weight. Residual moisture was measured by Karl Fischer titration with a Metrohm 684 KF coulometer (Brinkmann Instruments, Inc., Westbury, NY) and Hydranal reagents (Sigma-Aldrich Company, St. Louis, MO). Each titration consisted of injecting ~100 μl of either blank DMSO or a DMSO/lyophile solution into the titrator with constant stirring by using a 1 ml disposable plastic syringe (Becton, Dickinson

and Company, Franklin Lakes, NJ). The exact amount injected was determined by the difference in weight between the syringe before and after transferring the solution. The total amount of moisture in the lyophile was calculated by subtracting the amount of water in the DMSO from that measured in the DMSO/lyophile solution and calibrated using a standard curve obtained by adding known quantities of water to the Karl Fischer media. The percent of water content was calculated by multiplying by 100 the ratio of the amount of water determined to the amount of lyophile.

Powder X-ray Diffraction (PXRD)

Powder X-ray diffraction analyses of lyophiles produced from 20 mg/ml PVP solutions in 50 mM pH 4.0 and 6.0 phosphate buffer and lyophiles from solutions containing 5 mM CSH and 5 mM H_2O_2 in 20 mg/ml PVP with 50 mM pH 6.0 phosphate buffer were conducted to confirm their amorphous nature. Powder X-ray diffraction patterns of solid samples were determined at ambient temperature using a SIEMENS D500 X-ray powder diffractometer with Bragg-Brentano optics to accomplish focusing (Bruker AXS Inc., Madison, WI). Samples of amorphous solids were packed as a thin layer into an aluminum sample holder. Crystalline solids ($Na_3PO_4{\cdot}12H_2O$, $Na_2HPO_4{\cdot}7H_2O$, and $NaH_2PO_4{\cdot}H_2O$) were ground into fine powders using a mortar and pestle, transferred to the top of a quartz holder, and several drops of acetone were added to facilitate powder adhesion after the evaporation of acetone. Samples were exposed to Cu–K_α radiation at 40 kV and 30 mA. The scanning range of 2θ was from 10° to 60° with a step size of 0.05° and scanning rate of 1°/min.

Modulated Temperature Differential Scanning Calorimetry (MTDSC)

MTDSC analyses were carried out using a TA Instruments DSC2920 (TA Instruments Inc., New Castle, DE) with MTDSC capacity and refrigerated cooling system under a dry nitrogen purge. The samples (~5 mg) were hermetically sealed in aluminum sample pans and analyzed *versus* an empty pan in the reference oven. Samples were first equilibrated at 5°C, then heated from 5 to 260°C at 5°C/min. At the end of the heating process, the samples were cooled to 5°C at 10°C/min then reheated to 260°C at 5°C/min and thermal data were collected. During the heating and cooling processes, a modulation amplitude of ±0.5°C and a period of 40 s was used for each sample.

pH and Initial Reactant and Product Concentrations After Reconstitution

The pH of samples from several lyophile batches was measured immediately after reconstitution in 0.5 ml deionized water. Initial concentrations of both reactants (CSH and H_2O_2) and products were determined immediately after freeze drying by dissolving samples in 0.5 ml of a quench solution (50 mM phosphoric acid, 5 mM sodium 1-nonanesulphonate, and 5% acetonitrile in water) and then adding 0.5 ml DI water. Assays were carried out by HPLC as described below.

High-Performance Liquid Chromatography (HPLC)

The analyses of cysteine (CSH), cystine (CSSC), cysteine sulfinic acid (CSO_2H), cysteine sulfonic acid (CSO_3H) and hydrogen peroxide (H_2O_2) were carried out by reversed phase high performance liquid chromatography (HPLC). The system consisted of a Beckman 110A Solvent Delivery Module (Beckman Coulter, Fullerton, CA), a Waters 717 Plus Autosampler (Waters Corp., Milford, MA) and a Hewlett-Packard 1040M Series II HPLC detector (Hewlett-Packard Company, Palo Alto, CA) operating at 214 nm which was connected to a PC for data acquisition and analysis using HP LC/MSD ChemStation software. Two Supelcosil ABZ+Plus, 5 μm (250 × 4.6 mm) analytical columns (Supelco, Bellefonte, PA) in tandem and a 5 μm (2 cm×2.1 mm) guard column were employed. Elutions were performed isocratically at a flow rate 0.8 ml/min using a mobile phase consisting of 50 mM phosphoric acid, 2.5 mM Sodium 1-nonanesulphonate (99%, Lancaster Synthesis, Inc., Windham, NH), and 2.5% (v/v) acetonitrile in water adjusted to pH 2.15 with NaOH. The retention times for CSO_3H, CSO_2H, H_2O_2, CSH, and CSSC were ~6.5, ~6.8, ~7.5, ~17 and ~27.5 min, respectively.

General Procedure for Kinetic Studies

Vials containing lyophiles sealed under vacuum were placed in a controlled temperature chamber at 25°C. Initial (t_0) samples and samples at later time points were either assayed immediately after reconstitution or immediately frozen in liquid N_2 after reconstitution and stored under liquid N_2 prior to their analysis. Lyophiles were reconstituted by first dissolving them in 0.5 ml of a quench solution (50 mM phosphoric acid, 5 mM sodium 1-nonanesulphonate, and 5% acetonitrile in water) and then adding 0.5 ml DI water. Assays were carried out by HPLC as described above.

For the initial rate studies, samples were taken in the early stage of the reaction between CSH and H_2O_2. Typically, the initial rate region was considered to include the time frame during which less than 5% change in the concentration of CSH had occurred.

Data Analysis

Concentrations of CSH, H_2O_2, CSSC, CSO_2H, and CSO_3H in quenched lyophiles determined at different reaction times by HPLC analysis were converted to solid state concentrations (M). The volume of the solid was estimated from the calculated McGowan volumes (29) of all solid phase components. The McGowan volume of a single molecule is obtained from individual atom contributions using the following equations:

$$V_x = \sum \text{atom contributions} - \sum 6.56B \qquad (1)$$

$$B = N - 1 + Rg \qquad (2)$$

where V_x is the calculated McGowan volume of a molecule, B is the total number of bonds (single, double, or triple bonds each count as one), N is the total number of atoms, and Rg is the total number of ring structures. The primary contribution

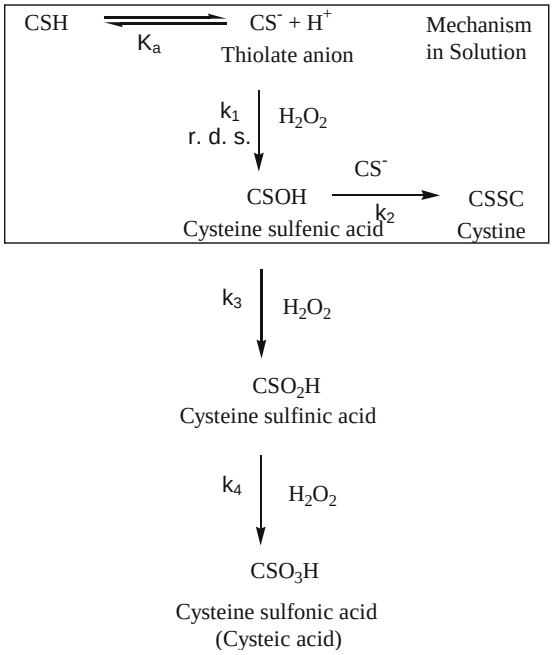

Scheme I. Proposed mechanism for the reaction of CSH and H_2O_2 in amorphous PVP lyophiles. The outlined portion represents the mechanism established for the reaction in aqueous solutions.

to the total volume of solid in the amorphous lyophiles is from PVP $\{(C_6H_9NO)_n$ where n = 3,243$\}$. Initial rates of product formation were obtained from the initial slopes of product concentration *versus* time curves. Reactant and product concentrations *versus* time in the initial rate region in lyophiles at each pH were also fit to a mathematical model (Eqs. 3–7), which was derived from Scheme I, using non-linear least squares regression analysis (SCIENTIST®, Micromath Inc., Salt Lake City, UT). Equations (3)–(7) were constructed to allow for the existence of two (or more) sub-populations of reactants (i subscripts in Eqs. (3)–(7) having different reactivities (k_i). Models based on Eqs. (3)–(7) assuming either homogeneous (i.e., a single reactant population) or heterogeneous kinetics (i.e., two reactant populations having different reactivities) were evaluated.

$$\frac{d[CSH]_i}{dt} = -k_{1i}[CSH]_i[H_2O_2]_i - k_{2i}[CSH]_i[CSOH]_i \quad (3)$$

$$\frac{d[H_2O_2]_i}{dt} = -k_{1i}[CSH]_i[H_2O_2]_i - k_{3i}[CSOH]_i[H_2O_2]_i - k_{4i}[CSO_2H]_i[H_2O_2]_i \quad (4)$$

$$\frac{d[CSOH]_i}{dt} = k_{1i}[CSH]_i[H_2O_2]_i - k_{2i}[CSH]_i[CSOH]_i - k_{3i}[CSOH]_i[H_2O_2]_i \quad (5)$$

$$\frac{d[CSSC]_i}{dt} = k_{2i}[CSH]_i[CSOH]_i \quad (6)$$

$$\frac{d[CSO_2H]_i}{dt} = k_{3i}[CSOH]_i[H_2O_2]_i - k_{4i}[CSO_2H]_i[H_2O_2]_i \quad (7)$$

RESULTS

Preparation and Characterization of Amorphous PVP Lyophiles containing CSH and H_2O_2

Shown in Table I are the initial and final compositions of the various lyophiles produced for the kinetic studies. Because CSH and H_2O_2 react rapidly in aqueous solution under the conditions employed in preparing solutions for

Table I. Composition of CSH and H_2O_2-Containing PVP Lyophiles used in Kinetic Studies

[CSH]:[H_2O_2] (CxHy)[a]	pH	C4H6	C4H3	C4H2	C4H1	C1H3	C2H3	C8H3	C4H4[c]
CSH initial (mM)		4.0	4.0	4.0	4.0	1.0	2.0	8.0	4.0
H_2O_2 initial (mM)		8.0	4.0	2.0	1.0	4.0	4.0	4.0	5.0
%CSH	4.0	96 ± 1[b]	96 ± 1	98 ± 2	100 ± 5	92 ± 0.4	91 ± 1	97 ± 1	–
remaining	6.0	89	90	92	95	84	87	92	93 ± 3
%H_2O_2	4.0	74 ± 3	76 ± 1	78 ± 4	75 ± 6	72 ± 4	74 ± 2	74 ± 2	–
remaining	6.0	88	94	101	113	90	92	89	80 ± 1
%CSSC formed	4.0	1.5 ± 0.1	1.5 ± 0.3	0.9 ± 0.2	0.9 ± 0.1	2.5 ± 0.6	1.7 ± 0.3	1.3 ± 0.1	–
	6.0	6.4	3.7	2.8	2.3	7.7	4.4	5.1	4.0 ± 0.5
%H_2O (w/w)	4.0	7.3 ± 0.5	8.2 ± 1.1	7.4 ± 1.3	6.4 ± 0.7	9.4 ± 1	8.6 ± 2	8.3 ± 0.3	–
	6.0	–	–	–	–	–	–	–	7.1 ± 0.7
Mass balance (%)	4.0	98 ± 1	97 ± 2	99 ± 2	101 ± 5	95 ± 0.1	93 ± 2	99 ± 1	–
	6.0	95	94	95	97	92	91	97	97 ± 3
$[CSH]_{lyophile}$ (M)	4.0	0.31 ± 0.004	0.31 ± 0.004	0.32 ± 0.005	0.34 ± 0.015	0.08 ± 0.001	0.15 ± 0.002	0.61 ± 0.006	–
	6.0	0.29	0.29	0.3	0.32	0.07	0.14	0.58	0.32 ± 0.01
$[H_2O_2]_{lyophile}$ (M)	4.0	0.48 ± 0.02	0.25 ± 0.004	0.13 ± 0.006	0.06 ± 0.005	0.24 ± 0.014	0.24 ± 0.008	0.23 ± 0.002	–
	6.0	0.57	0.31	0.17	0.09	0.3	0.3	0.28	0.34 ± 0.01

[a] CxHy reflects composition (mM) of reconstituted lyophiles (to their original volumes)
[b] ± Values reflect standard deviations (n = 3); otherwise n = 1
[c] All formulations but C4H4 were used for initial rate studies. The C4H4 formulation was used to generate complete concentration *versus* time data over 100 h.

lyophilization (28) and because H_2O_2 has a significant vapor pressure (30), special precautions were necessary to minimize degradant formation and loss of H_2O_2. First, solutions of CSH and H_2O_2 had to be prepared separately, mixed rapidly, and quick-frozen in a liquid N_2 bath. Secondly, the primary drying process was conducted at −45°C and secondary drying was eliminated to prevent degradation prior to the initiation of kinetic studies at 25°C and to minimize loss of H_2O_2. These precautions enabled the production of lyophiles at pH 4.0 containing <5% CSSC formation (Table I). Since CSSC does not participate significantly in the reactions investigated in Scheme I (*vide infra*), such formulations were considered suitable as model formulations for kinetic studies. Generally, a lower pH (i.e., pH 4.0) produced formulations with less initial CSSC formation. Consequently, formulations at pH 4.0 were emphasized in the initial rate studies. Lower reactant concentrations also provided formulations with reduced degradant formation, but lower concentrations increased the time required for kinetic studies and made the analyses of initial rates of product formation more difficult.

The drying procedure employed also enabled the retention of most of the H_2O_2 initially added (~75%) while removing most of the water. Since the concentrations of H_2O_2 present in lyophiles at t_0 were determined by HPLC, some loss during freeze-drying was inconsequential. Average moisture contents determined by Karl Fischer titration ranged from ~6–10% and were independent of the [CSH]:[H_2O_2] ratio.

The pH values of reconstituted solutions from several lyophile batches indicated no change in pH from the solutions that were lyophilized (pH of reconstituted lyophiles averaged 4.01 ± 0.01 (n = 2) and 6.00 ± 0.01 (n = 15), respectively). In this paper, the term 'pH' refers to a lyophile property. It is the pH that lyophiles produce after reconstitution, which may not be the same value as the effective pH in the amorphous solid.

Comparisons of the powder X-ray diffraction patterns of lyophiles prepared from solutions containing 20 mg/ml PVP in 50 mM pH 6.0 phosphate buffer either with or without CSH and H_2O_2 (each at 5 mM) to those for several crystalline powders of phosphate salts ($Na_3PO_4 \cdot 12H_2O$, $Na_2HPO_4 \cdot 7H_2O$, $NaH_2PO_4 \cdot H_2O$) revealed no evidence of crystallization of phosphate salts either initially or during storage for 7 days at 25°C, which is consistent with previous evidence that the presence of various glass-forming excipients inhibits the crystallization of phosphate salts (31).

MTDSC was employed to detect the glass transition temperatures (T_g) of both pure PVP and an amorphous PVP lyophile prepared from 20 mg/ml PVP in 50 mM pH 6.0 phosphate buffer containing 5 mM CSH and 5 mM H_2O_2. The value of T_g estimated for pure PVP was 183.6°C on heating and 179°C on cooling, which is consistent with the literature values (16,32). The value of T_g estimated for an amorphous PVP lyophile prepared from 20 mg/ml PVP in 50 mM pH 6.0 phosphate buffers containing 5 mM CSH and 5 mM H_2O_2 and stored at 25°C for 1 week was 182.3°C on heating and 180.4°C on cooling, indicating that the glass transition temperature of the amorphous PVP lyophile was similar to that of pure PVP and well above the temperature (25°C) at which solid-state kinetic studies were conducted. No evidence of other phase transitions was found by the MTDSC analyses.

HPLC Analysis of Reactant Disappearance and Product Formation in the Reaction of CSH and H_2O_2 in Amorphous Solids

Previously, an HPLC method was developed to simultaneously monitor the disappearance of CSH and H_2O_2 and the appearance of CSSC, the primary solution degradant, in a kinetic study in aqueous buffers as a function of reactant concentrations and pH (28). Although UV detection at 214 nm is less sensitive than electrochemical detection for H_2O_2 (33) and for CSH and CSSC (34) it is more stable and convenient. Cysteine sulfinic acid CSO_2H and sulfonic acid CSO_3H were not observed in the solution reaction except at

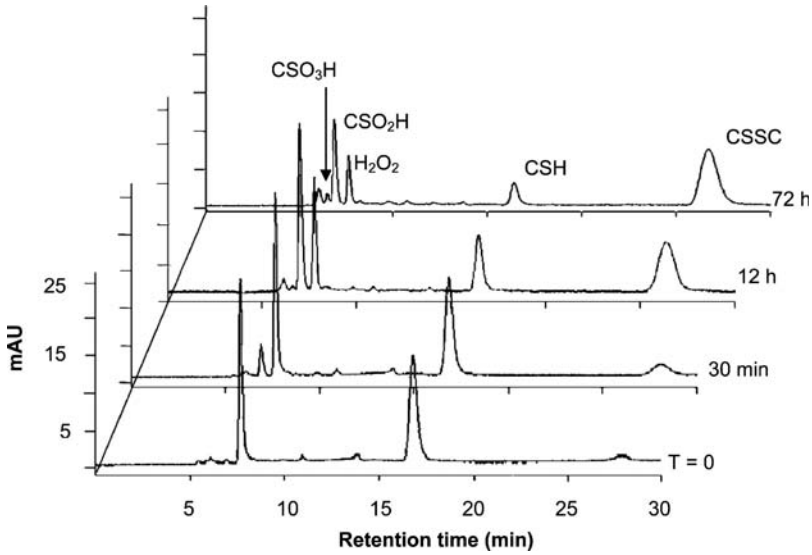

Fig. 1. HPLC chromatograms (214 nm) generated at various times during the reaction of CSH with H_2O_2 in amorphous PVP lyophiles at 25°C. Lyophiles were prepared from solutions containing 10 mg/ml PVP, 2 mM CSH, and 4 mM H_2O_2 in 50 mM pH 6.0 phosphate buffer.

very high ratios of H_2O_2 to CSH, but they were detected in amorphous PVP lyophiles, necessitating the development of an HPLC method that would allow the simultaneous analysis of CSO_3H, CSO_2H, CSH, H_2O_2 and CSSC. Separations of CSO_2H from CSO_3H required two Supelcosil ABZ+Plus columns connected in series and a flow rate of 0.8 ml/min. Under these conditions, retention times for CSO_3H and CSO_2H were ~6.5 and ~6.8 min, respectively.

Linearity in the HPLC response factors was established over the concentration ranges of 100 μM–10 mM for CSH and H_2O_2, 4 μM–3 mM for CSSC, 0.5 μM–2.5 mM for CSO_2H, and 150 μM–90 mM for CSO_3H with intraday coefficients of variation of <1.5% for all analytes except H_2O_2 for which the coefficient of variation was 3.3%. The response factor for CSO_3H was only 1.4% of that for CSO_2H, which limited the ability to monitor the formation of CSO_3H in the early stages of the reaction.

Figure 1 displays typical HPLC chromatograms for reconstituted amorphous PVP lyophiles containing CSH and H_2O_2 (prepared from pH 6.0 phosphate buffer) *versus* lyophile storage time at 25°C. A comparison of these chromatograms with those generated for the same reactions in solution revealed the formation of two new product peaks corresponding in their retention times and UV spectra to CSO_3H (peak eluting earlier) and CSO_2H in addition to the peak for CSSC.

Reconstituted samples in quench solution were sufficiently stable to enable analyses of both reactant disappearance and product formation simultaneously using this HPLC method. Figure 2A displays plots for the disappearance of CSH and H_2O_2 *versus* time in amorphous PVP lyophiles stored at 25°C while Fig. 2B shows the concentrations of CSSC, CSO_2H, and CSO_3H forming in the same lyophiles, which were prepared from 10 mg/ml PVP, 4 mM CSH and 5 mM H_2O_2 in 50 mM pH 6.0 phosphate buffer solutions. Qualitatively, Fig. 2 illustrates the increased importance of reaction pathways leading to the formation of CSO_3H and CSO_2H in the amorphous solid-state reaction.

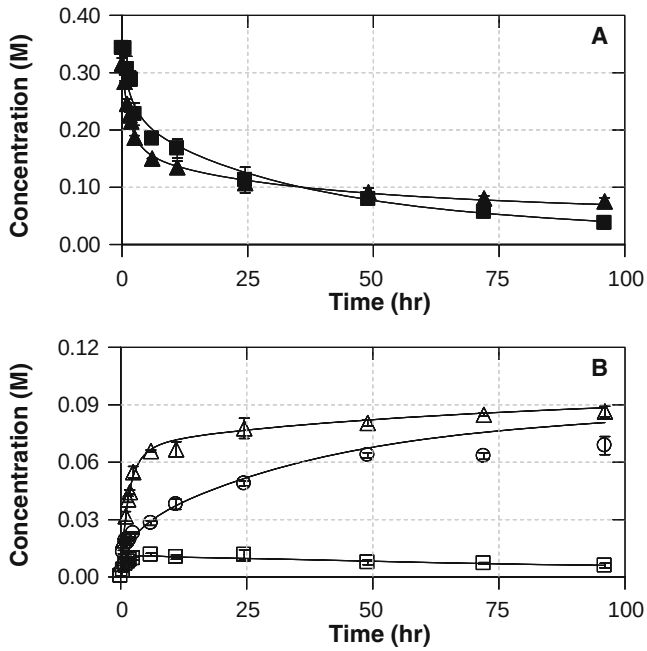

Fig. 2. Reactant (CSH, ▲; H_2O_2, ■) disappearance and degradant (CSSC, △; CSO_2H, □; and CSO_3H, ○) formation in amorphous PVP lyophiles at 25°C. Lyophiles were prepared from solutions containing 10 mg/ml PVP, 4 mM CSH, and 5 mM H_2O_2 in 50 mM pH 6.0 phosphate buffer. *Solid lines* reflect the best fit using Eqs. (3)–(7) with $i = 2$ (see also Table IV).

Kinetic Studies of the Reaction of CSH with H_2O_2 in Amorphous PVP

To ensure that the products forming in the amorphous lyophiles involve only the reaction of CSH with H_2O_2, preliminary experiments were carried out to determine the stability of CSH and H_2O_2 alone in amorphous PVP. Both were found to be stable (no significant change in concentration) in PVP at 25°C over the time frame (100 h) of the longest kinetic studies. The stability of CSSC in amorphous PVP both in the presence and absence of H_2O_2 at 25°C was also determined. While no reaction occurred in the absence of H_2O_2, a gradual decline in CSSC could be detected over several hundred hours in the presence of H_2O_2 which could be fit to a linear equation (% of CSSC remaining = $-0.0492*t$ + 99.823, $R^2 = 0.9997$, where t is time (h)). While this reaction would have a negligible effect on the initial rate studies, which were typically conducted over a 30-min time frame, it could impact long-term kinetic studies such as that shown in Fig. 2. However, the extent of decomposition of CSSC in the presence of H_2O_2 was <5% at 100 h, so even in the time frame explored in Fig. 2 this reaction would have only a minor contribution. Two well-resolved product peaks were observed from this reaction, both eluting at retention times of ~15 min. These product peaks were not significant in chromatograms generated in the kinetic studies of the reaction of CSH and H_2O_2.

Initial rate studies of the reaction between CSH and H_2O_2 were conducted at 25°C in amorphous PVP lyophiles prepared from 10 mg/ml PVP in 50 mM pH 4.0 ($n = 3$) or pH 6.0 ($n = 1$) phosphate buffer as described in Table I. These formulations varied either in their initial concentration of CSH ($[CSH]_0$ = 1, 2, 4, 8 mM (after lyophile reconstitution)) at constant H_2O_2 concentration (3 mM) or in their initial concentration of H_2O_2 ($[H_2O_2]_0$ = 1, 2, 3, and 6 mM (after lyophile reconstitution)) at a constant CSH concentration (4 mM). Also listed in Table I are the calculated molar concentrations of CSH and H_2O_2 in the lyophiles. The concentrations of the two major degradants forming in the initial rate region, CSSC and CSO_2H, are plotted *versus* time in Fig. 3. Initial rates of formation of each product for each set of reactant concentrations were generated from the slopes of the concentration *versus* time curves in the region corresponding to <5% change in CSH concentration at pH 4.0 (<10% change in CSH at pH 6.0).

Several significant features are evident in Fig. 3. First, the initial rates of formation of both products increase with an increase in CSH concentration at fixed H_2O_2 concentration or with an increase in H_2O_2 concentration at a fixed concentration of CSH, indicating that the rate determining step in the reaction depends on the concentrations of both reactants. Second, the rate of CSSC formation exceeds that

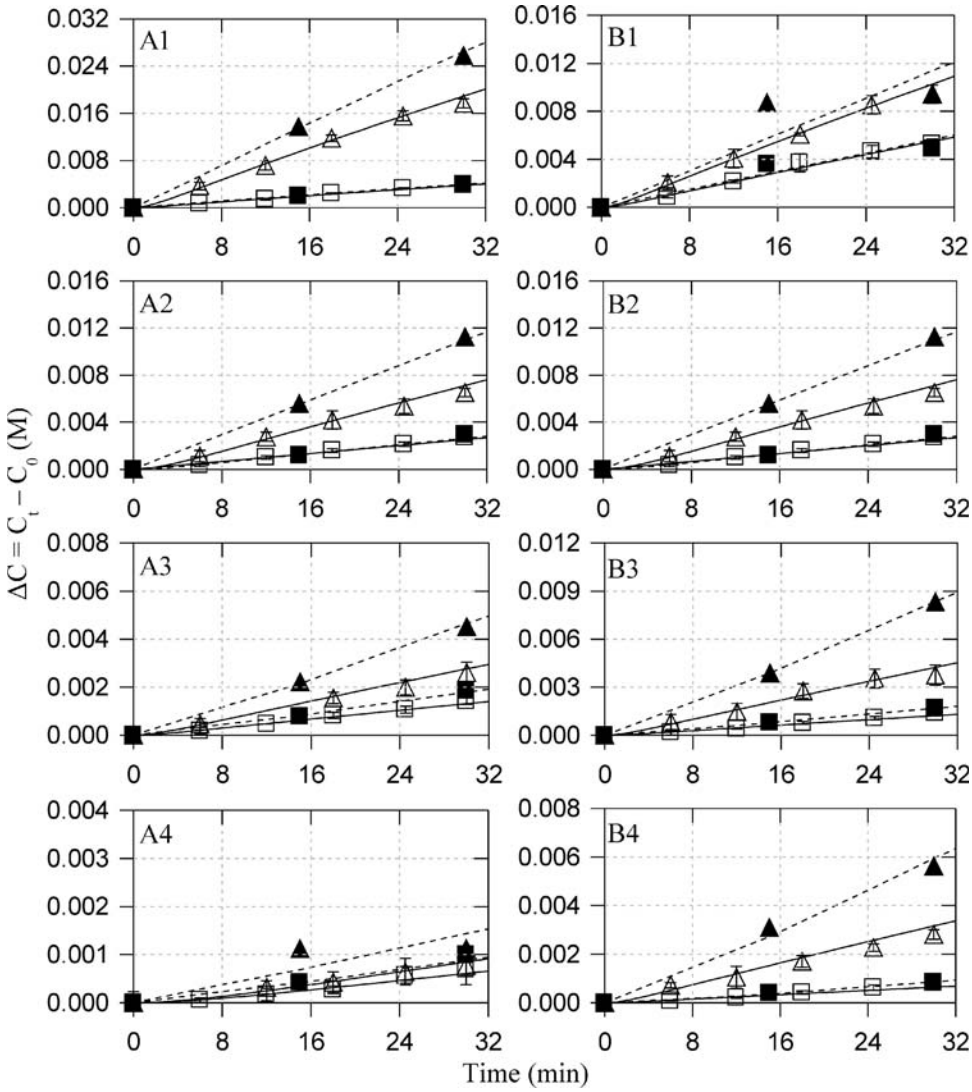

Fig. 3. Initial rates of formation of CSSC (△, ▲) and CSO_2H (□, ■) in lyophiles prepared from pH 4 (△, □) or pH 6 (▲, ■) buffers. *Left panel*: $[H_2O_2]_0$ fixed at 3 mM and $[CSH]_0$ = 8, 4, 2, 1 mM (A1–A4). *Right panel*: $[CSH]_0$ fixed at 4 mM and $[H_2O_2]_0$ = 6, 3, 2, 1 mM (B1–B4). *Dash lines* are the model fitted (Eqs. 3–7, i = 1) curves for 'pH 6' data and *solid lines* are the fitted curves for 'pH 4' data. Here C_t and C_0 are the concentration in the lyophiles at time t and time 0 respectively.

for the formation of CSO_2H at low $[H_2O_2]$:[CSH], while CSO_2H formation becomes more significant at high $[H_2O_2]$:[CSH] concentration ratios. This is more clearly illustrated in Fig. 4, where the percent of CSSC or CSO_2H in the total product are plotted *versus* the initial concentrations of CSH at fixed $[H_2O_2]$ (upper panels) or *versus* the initial concentrations of H_2O_2 at fixed [CSH] (lower panels). Finally, the initial rates of degradant formation (Fig. 3) appear to be nearly independent of pH between 4.0 and 6.0 while percent of CSSC in the total decomposition product mixture (Fig. 4) increased modestly at pH 6.0 (right panel) compared to pH 4.0 (left panel).

Recognizing that in solution the reaction of CSH with H_2O_2 produces a reactive intermediate (CSOH), the formation of which is rate-determining, the apparent reaction order was examined by summing the initial rates of CSSC and CSO_2H formation rather than considering each product individually. Shown in Fig. 5 are plots of log ($d[CSSC]/dt + d[CSO_2H]/dt$) *versus* the logarithms of the initial concentrations of either CSH or H_2O_2. From the slopes of these log–log plots, the apparent reaction order with respect to each reactant could be determined. Also shown in Fig. 5 are the log (initial rate) *versus* log (concentration) plots obtained for CSSC formation in aqueous solutions containing CSH and H_2O_2 generated in a previous study (28). Whereas the solution reaction exhibited apparent reaction orders (i.e., slopes) very close to 1.0 with respect to both CSH and H_2O_2, Fig. 5 suggests more complex relationships in amorphous PVP. Linear regression analyses of the data at 'pH 4' generated Eq. (8), which again suggests a more complex dependence of the initial rates on reactant concentrations in amorphous PVP, at least with respect to H_2O_2 concentration, than in solution. Similar reaction orders were observed at 'pH 6.'

$$\{d[CSSC]/dt + d[CSO_2H]/dt\} = k_{CSO2H+CSSC} \times [CSH]_0^{1.27} \times [H_2O_2]_0^{0.76} \quad (8)$$

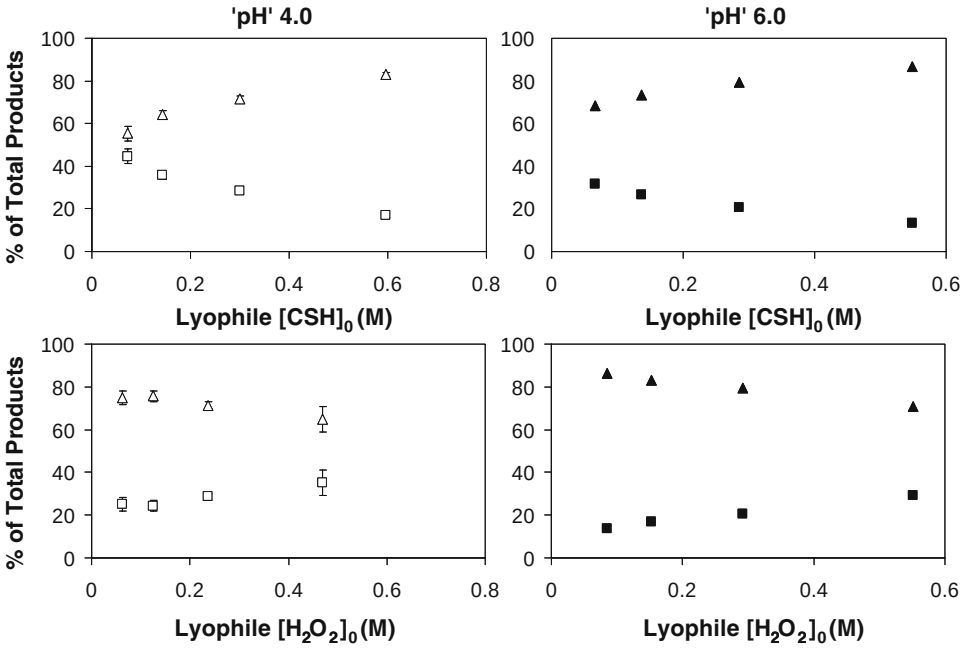

Fig. 4. Percent of total degradant accounted for by CSO_2H (□, ■) and CSSC (△, ▲) formation in the initial rate region of the reaction of CSH and H_2O_2 as a function of initial lyophile concentration of CSH or H_2O_2 in amorphous PVP lyophiles at 'pH 4.0' (*open symbols*) and 'pH 6.0' (*closed symbols*) and 25°C.

Kinetic Modeling of the Initial Rate Data Generated in Amorphous PVP

The appearance of CSO_2H and CSO_3H as significant degradants in addition to CSSC in the reaction of CSH with H_2O_2 in amorphous PVP suggested that the mechanism previously established for the reaction in aqueous solution, which produced only CSSC, had to be modified. Scheme I represents the proposed mechanism that was tested in this study. Initially, Eqs. (3)–(7) (ignoring the formation of CSO_3H in the initial rate region) were used to fit each set of reactant and product concentration *versus* time profiles shown in Fig. 3. Although this approach produced excellent fits, the parameter values k_2 and k_3 were highly correlated with each other, resulting in large 95% confidence limits for each. Significantly reduced correlation between the parameter values was obtained by substituting for k_2 and k_3 transforms reflecting the sum of $k_2 + k_3$ (i.e., k_{total}) and the fraction of CSOH converting to CSSC (i.e., $fd = k_2/(k_2 + k_3)$). This approach provided identical fits and clearly indicated

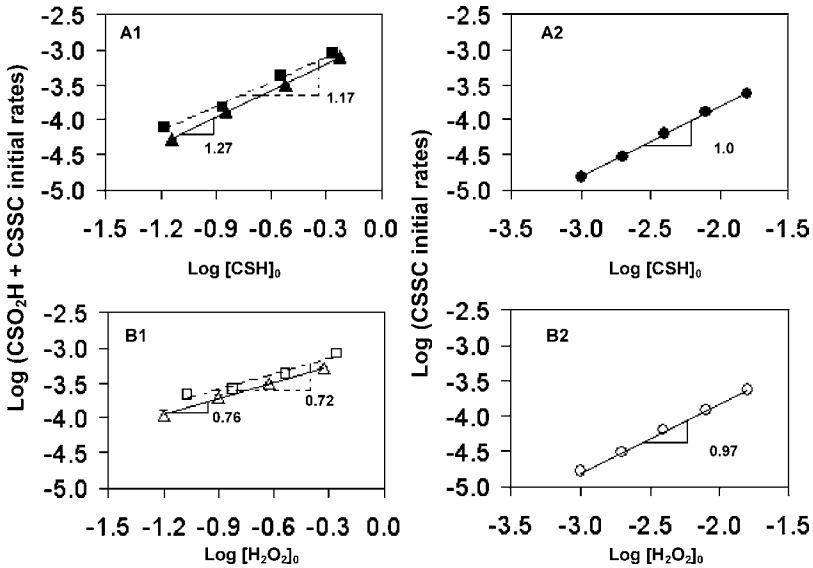

Fig. 5. Log–log plots of the initial rates of total product formation *versus* the starting concentrations of CSH (A) or H_2O_2 (B) in amorphous PVP lyophiles (*left panels*) or aqueous solution (*right panels*) at 25°C. Lyophiles were prepared from pH 4 (——, n = 3) or pH 6 (- - -, n = 1) buffers while aqueous solutions were at pH 6.0.

Table II. Parameter Values Generated from Fitting Scheme I to the Initial Rate Data* in Amorphous PVP at 'pH 4.0' and 'pH 6.0'

	k_1 ($M^{-1}min^{-1}$) ± 95% conf. limits		$k_2/(k_2 + k_3)$ ± 95% conf. limits		$k_2 + k_3$ ($M^{-1}min^{-1}$) ± 95% conf. limits	
Formulation	'pH 4'	'pH 6'	'pH 4'	'pH 6'	'pH 4'	'pH 6'
C8H3	0.0061 ± 0.0001	0.0056 ± 0.0002	0.65 ± 0.01	0.76 ± 0.004	1.6 ± 0.2	2.4 ± 1.8
C4H3	0.0049 ± 0.0001	0.0045 ± 0.0003	0.68 ± 0.01	0.81 ± 0.01	1.4 ± 0.2	2.7 ± 2.6
C2H3	0.0041 ± 0.0004	0.0044 ± 0.0002	0.78 ± 0.02	0.85 ± 0.004	3.3 ± 1.6	1.8 ± 0.4
C1H3	0.0034 ± 0.0003	0.0042 ± 0.0013	0.82 ± 0.01	0.92 ± 0.03	1.7 ± 0.3	13.9 ± ND**
C4H6	0.0039 ± 0.0001	0.0061 ± 0.0003	0.75 ± 0.01	0.83 ± 0.001	2.5 ± 0.6	1.3 ± 0.4
C4H2	0.0048 ± 0.0002	0.0080 ± 0.0002	0.57 ± 0.01	0.72 ± 0.004	2.8 ± 0.8	1.4 ± 0.2
C4H1	0.0067 ± 0.0007	0.0092 ± 0.0006	0.47 ± 0.03	0.67 ± 0.01	3.4 ± 2.3	1.3 ± 0.5

*Actual reactant and product molar concentrations in lyophiles rather than concentrations in reconstituted solutions were used to generate the above values.
**ND—95% confidence limits equal or exceed the parameter value.

that the uncertainty in parameter estimates was mostly associated with the overall rate of conversion of CSOH to products, k_{total}, while the ratios of products forming as reflected in $k_2/(k_2 + k_3)$ were well determined. The solid and dashed lines shown in Fig. 3 represent these best fits. Values of the parameters generated for each formulation are listed in Table II along with statistical information for each parameter. Clearly, the model was capable of fitting each data set when treated separately, supporting the hypothesis that Scheme I is an appropriate model for the solid-state reaction.

Because the formation of the reactive intermediate (CSOH) is the slow step in amorphous PVP, indicated in Table II by the fact that k_{total} exceeds k_1 by at least two orders of magnitude, the model based on Scheme I predicts that the overall initial reaction rate in amorphous PVP should be first order with respect to both CSH and H_2O_2 concentrations. Contrary to this expectation, as illustrated in Fig. 5, apparent reaction orders of 0.76 and 1.27 ('pH 4') and 0.72 and 1.17 ('pH 6') were obtained for the dependence of the initial rates on H_2O_2 and CSH, respectively.

A closer inspection of the parameter values in Table II reveals additional quantitative inconsistencies. The mean values (± SD) for k_1, $k_2/(k_2 + k_3)$, and $k_2 + k_3$ from Table II at pH 4.0 were 0.0048 ± 0.0012 $M^{-1}min^{-1}$, 0.67 ± 0.14, and 2.4 ± 0.8 $M^{-1}min^{-1}$, respectively. While the overall variability in these parameters does not seem large, the 95% confidence limits for k_1 and $k_2/(k_2 + k_3)$ for each formulation indicated significant differences between formulations. Bar graphs comparing the values of k_1 and $k_3/(k_2 + k_3)$ (= 1 − $k_2/(k_2 + k_3)$) in different formulations along with error bars reflecting their 95% confidence limits at both 'pH 4' and 'pH 6' are

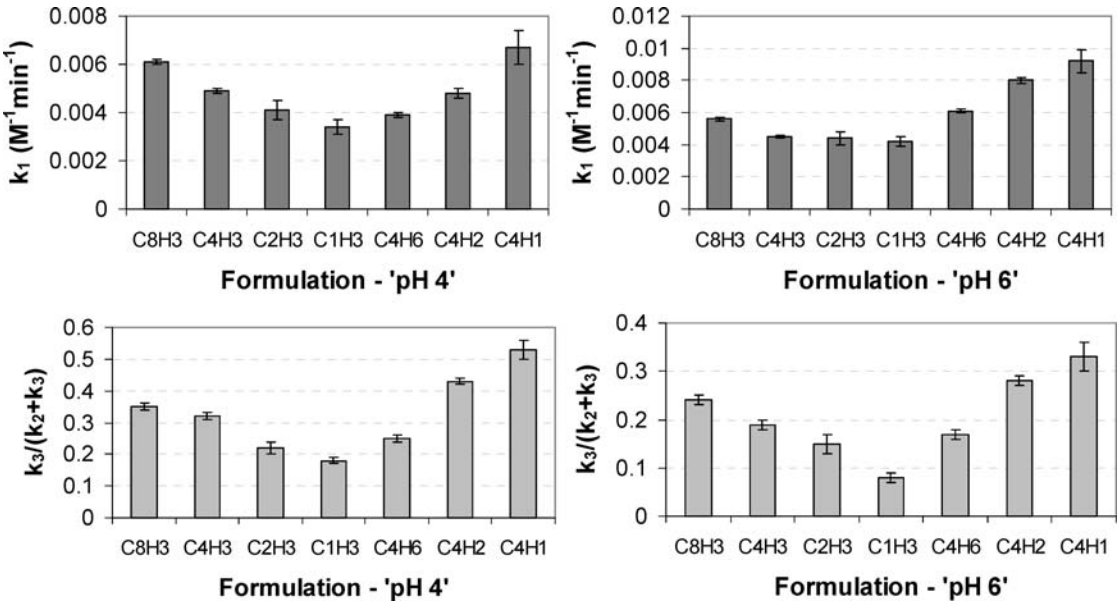

Fig. 6. Systematic variation in k_1 (*upper panels*) and $k_3/(k_2 + k_3)$ (*lower panels*) at 'pH' 4 (*left*) and 'pH' 6 (*right*) as the ratio of CSH and H_2O_2 in lyophile formulations is varied.

shown in Fig. 6. These comparisons clearly indicate significant and similar trends in the parameter values with varying CSH:H_2O_2 concentration ratios in the formulations at both pH values. A further analysis of the parameter values at pH 4 suggested linear relationships between these parameter values and X_{HOOH}, where X_{HOOH} is the mole fraction of H_2O_2 relative to the total moles of reactant (i.e., $X_{HOOH} = [H_2O_2]/([H_2O_2] + [CSH])$. Thus, at pH 4, $k_1 = -0.0051*X_{HOOH} + 0.0072$ ($r^2 = 0.8412$) and $k_2/(k_2 + k_3) = 0.5538*X_{HOOH} + 0.4202$ ($r^2 = 0.9424$). These empirical relationships between the rate constant parameters and formulation composition with respect to H_2O_2 provided an empirical model that could fit the entire data set (i.e., all compositions) at each pH.

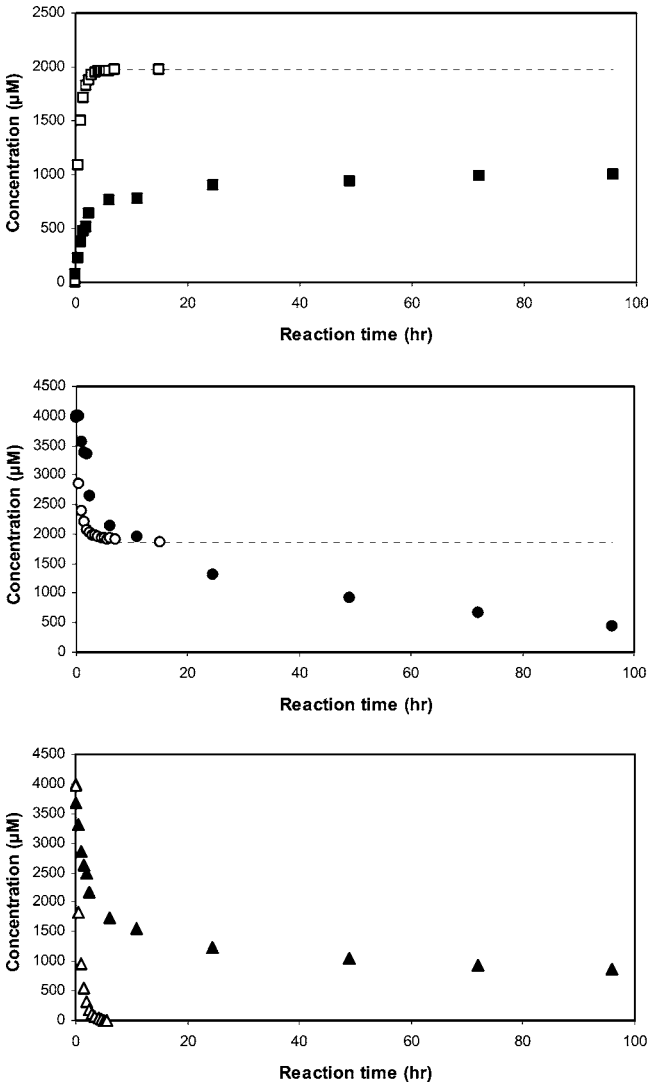

Fig. 7. Comparison of the reactions of cysteine and hydrogen peroxide in aqueous solution and in amorphous PVP (concentrations expressed are after reconstitution) at 25°C. Aqueous solutions contained 4 mM CSH and 4 mM H_2O_2 in 50 mM pH 6.0 phosphate buffer solutions. Amorphous PVP lyophiles contained (after reconstitution to their original volume) the same concentrations of CSH and H_2O_2 in 50 mM pH 6.0 phosphate buffer along with 10 mg/ml PVP. *Upper panel*, CSSC (■, □); *middle panel*, H_2O_2 (*P*, ○); and *lower panel*, CSH (▲, △)-aqueous solutions (*open symbols*); amorphous PVP (*closed symbols*).

Heterogeneous Dynamics Exhibited in Amorphous PVP

The reaction of CSH and H_2O_2 at 25°C in amorphous PVP lyophiles containing (after reconstitution to their original volume) 4 mM CSH and 4 mM H_2O_2 in 50 mM pH 6.0 phosphate buffer along with 10 mg/ml PVP was compared in Fig. 7 to the same reaction in aqueous solutions also containing 4 mM CSH and 4 mM H_2O_2 in 50 mM pH 6.0 phosphate buffer. Figure 7 demonstrates that the disappearance of the reactants and formation of products for the reaction of 4 mM CSH and 4 mM H_2O_2 is more rapid in aqueous solution at this pH than in amorphous PVP (at the same concentrations after reconstitution), despite the fact that the concentrations in amorphous PVP prior to reconstitution are significantly higher (~100-fold, Table I). In the solution reaction, two molecules of CSH are consumed for each molecule of H_2O_2 resulting in a rapid depletion of CSH from the solution (lower panel), producing CSSC as the only product (upper panel), and leaving unreacted H_2O_2 in solution. As noted previously, CSSC is only one of several products forming in amorphous PVP, though it is the only one shown in Fig. 7. The most remarkable difference between the solution and amorphous solid reactions illustrated in Fig. 7 is the nearly complete arrest of the decline in CSH after an initially rapid phase lasting approximately 5 h, leaving ~40–50% unreacted CSH which then gradually declines over the remaining reaction time to less than 25% remaining after 100 h. At the start of this slow decline phase in the decomposition of CSH approximately 1/2 of the original H_2O_2 concentration remains. The sudden slowing in the rate of decomposition of CSH (lower panel) is accompanied by a similar abrupt slowing in the rate of formation of CSSC (upper panel).

Two models were explored to fit the apparent biphasic character of the reaction in amorphous PVP. Each of the concentration *versus* time curves can be described individually by the Kohlrausch-Williams-Watts (KWW) stretched exponential equation (35–37) (Eq. 9):

$$\phi_{kww}(t) = \exp\left[-(t/\tau)^{\beta}\right] \tag{9}$$

where ϕ_{kww} (t) is a relaxation function (e.g., [CSH]/[CSH]$_o$, etc.), τ (> 0) is a relaxation time and β is a stretching parameter between 0 and 1 necessary to describe non-mono-exponential behavior. The parameters generated from fits of each concentration-time profile, shown in Fig. 8, are displayed in Table III. Understandably, different parameter values are obtained depending on the probe selected to monitor the process.

Alternatively, the simplest model that can account for the apparent biphasic character of the reaction in PVP that is also consistent with Scheme I assumes the existence of two populations of reactants having different kinetics (i.e., $i = 2$ in Eqs. 3–7). For first-order decay this would lead to a bi-exponential equation. This model has the advantage of enabling all of the reactant and product concentration *versus* time curves to be fit simultaneously. The solid lines in Figs. 2A and 2B were generated from this model and values for the reaction parameters are shown in Table IV. As judged by the excellent fit of the data in Fig. 2, a simple two population model with approximately 50–50 populations of

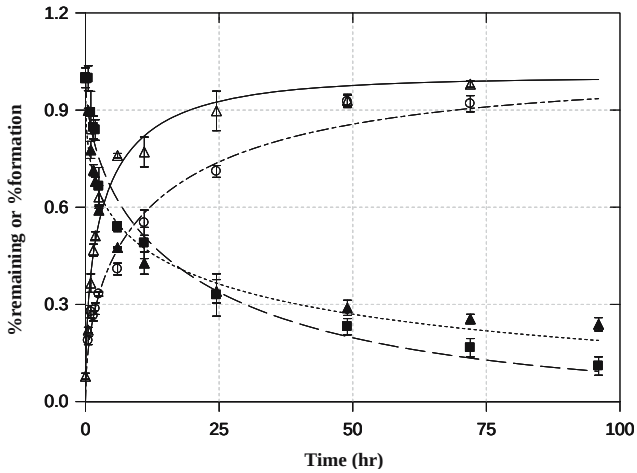

Fig. 8. Best fits of the KWW equation to each reactant (CSH (▲) and H_2O_2 (■)) and degradant (CSO_3H (○) and CSSC(△)) concentration *vs.* time profile during the reaction of CSH and H_2O_2 in amorphous PVP lyophiles prepared from 50 mM pH 6.0 phosphate buffer containing 10 mg/mL PVP, 4 mM CSH and 5 mM H_2O_2.

reactants differing by ~ one order-of-magnitude in reactivity is adequate for this set of conditions.

DISCUSSION

Many important degradation pathways affecting pharmaceutical products involve formation of a reactive intermediate along the reaction coordinate. Considering only reactions prevalent in peptide and protein formulations, deamidation, isomerization, and racemization reactions at asparagine and glutamine residues proceed through a cyclic imide intermediate (38); peptide bond cleavage at aspartate residues may involve a cyclic anhydride intermediate; in some instances cyclic anhydride formation may produce covalent, amide-linked aggregates (39–41); covalent aggregates may also form from reactive free thiol intermediates which are generated from disulfide bond hydrolysis and can participate in thiol-disulfide exchange reactions (42–44); finally, the Maillard reaction between amine-containing molecules and reducing sugar excipients involves a Schiff base intermediate (45). The kinetics of such reactions, which involve multiple steps, may be more complicated in the solid-state due to the more limited molecular mobility of the participants in the various stages of a reaction. Because of this and other complicating factors, kinetic models based on reaction mechanisms originally developed for solutions generally fail to account for reactivity in the solid-state (1,45). Nevertheless, knowledge of the existence of a reactive intermediate may be instrumental in rationalizing and ultimately predicting differences in reaction kinetics and degradant profiles in amorphous solid-state reactions.

We and others have demonstrated (25–28) that the reaction between thiols and hydrogen peroxide in aqueous solution (in the absence of metal ions) involves bimolecular nucleophilic attack of thiolate to form a reactive sulfenic acid intermediate (RSOH), ultimately producing a disulfide (RSSR) via reaction of the intermediate with a second thiol molecule as described in Scheme I (section outlined). An alternative pathway for the sulfenic acid intermediate through further reaction with H_2O_2 can occur (46), which is also described in Scheme I, leading to a sulfinic acid (RSO_2H) and ultimately to a sulfonic acid (RSO_3H) but in aqueous solution these reactions appear to be unimportant except possibly at extremely high ratios of H_2O_2 (25–28).

Intuitively, one might expect that in an amorphous PVP glass the bimolecular reaction between CSOH and CSH (or CS^-), the fast (i.e., non-rate-determining) reaction step in solution, might be substantially reduced given the restricted translational mobility in glassy polymers due to their high viscosities below T_g (18). For a reaction which is molecular mobility or diffusion controlled, relative rate constants are often estimated by the Stokes-Einstein equation (Eq. 10) which relates the translational diffusion coefficient, D_t, to the inverse of viscosity (η) and molecular radius (r) (13,45,47):

$$D_t = \frac{k_b T}{6\pi\eta r} \tag{10}$$

Recent molecular dynamics simulations of small molecule diffusion in amorphous PVP glass suggest that the size selectivity for solute diffusion may be significant (19,24). A simulation of the diffusion coefficients of water and a tripeptide in both bulk water and in glassy PVP indicated that whereas the self-diffusion coefficient for water in bulk water was 370-fold greater than in PVP, the diffusion of the tripeptide in water exceeded its value in PVP by 3,700-fold.

If the reactions in Scheme I become mobility-controlled in amorphous PVP, the substantially reduced diffusion coefficients for CSH and CSOH increase the likelihood for the alternate pathway for reaction of CSOH with the smaller (and more mobile) molecule, H_2O_2. Indeed, this anticipated outcome is observed, as demonstrated by the HPLC chromatograms in Fig. 1 and the product concentration *versus* time profiles in Fig. 2, both of which demonstrate the formation of three significant degradation products in the reaction between CSH and H_2O_2 in amorphous PVP. The disulfide, CSSC, the predominant product in aqueous solution is also the major decomposition product in amorphous PVP but significant quantities of

Table III. Parameter Values Generated from Fitting the KWW Equation (Eq. 9) to each Concentration *vs.* Time Profile in Fig. 8

	Sum of squared deviations	Model selection criterion (MSC)	τ (95% conf. limits)	β (95% conf. limits)
CSH	0.0297	2.877	24.1 (12.9, 35.3)	0.37 (0.27, 0.47)
H_2O_2	0.0342	3.2071	21.7 (13.9, 29.5)	0.58 (0.44, 0.73)
CSSC	0.0266	3.1517	3.8 (2.4, 5.2)	0.51 (0.34, 0.68)
CSO_3H	0.0153	3.4066	14.2 (9.8, 18.6)	0.53 (0.42, 0.64)

Table IV. Parameter Values Generated by Simultaneously Fitting Eqs. (3)–(7) ($i = 2$) to All of the Concentration* *vs.* Time Profiles in Fig. 2

	k_1 ($M^{-1}min^{-1}$) ± 95% conf. limit	$k_2/(k_2 + k_3)$ ± 95% conf. limit	$k_2 + k_3$ ($M^{-1}min^{-1}$) ± 95% conf. limits	k_4 ($M^{-1}min^{-1}$) ± 95% conf. limits	$Fx = [a]/([a] + [b])$ ± 95% conf. limits
Population a	0.044 ± 0.009	0.8 ± 0.01	0.31 ± 0.06	0.06 ± 0.01	0.52 ± 0.023
Population b	0.001 ± 0.0001	0.25 ± 0.06	0.009 ± 0.003	0.015 ± 0.002	

*Molar concentrations of reactants and products in lyophiles.

CSO_3H are also found. CSO_2H formation is important in the initial stages of the reaction but it degrades further to CSO_3H. This change in degradant profile is the first line of evidence in support of the hypothesis that the reaction in amorphous PVP proceeds through the same reactive intermediate but to produce a more diverse array of products due to the increased importance of translational (and possibly rotational) diffusion in the solid-state reaction.

Initial rate studies conducted at 'pH 4.0' and 'pH 6.0' and at varying ratios of [CSH]:[H_2O_2] provide further evidence for the hypothesis that the reaction in amorphous PVP is governed by Scheme I. The plots for the initial rates of formation of CSSC and CSO_2H illustrated in Fig. 3 show the following features consistent with Scheme I: (1) the overall reaction rate and the rates of formation of both degradants increase with increasing concentrations of either CSH or H_2O_2 indicating that the rate law must include the concentrations of both; (2) CSSC and CSO_2H formation rates *both* increase with *either* an increase in CSH or an increase in H_2O_2, consistent with the initial formation of a reactive intermediate (e.g., the rate of CSSC formation would not be expected to increase with an increase in H_2O_2 unless an intermediate were involved); (3) both degradants form in parallel with no apparent lag time, suggesting that the reactive intermediate formation is rate-determining (i.e., no significant build-up in concentration of intermediate); (4) the ratios of initial rates of formation of CSSC and CSO_2H vary in response to the initial concentrations of CSH and H_2O_2 in the expected manner (qualitatively) for a reaction in which the two reactants are competing for the same intermediate, as more clearly shown in Fig. 4 (i.e., the percent of total degradant accounted for by CSSC increases with increasing CSH/H_2O_2 while CSO_2H accounts for a higher percentage of the total with increasing H_2O_2/CSH); and (5) the absence of detectable levels of CSO_3H suggests that CSO_2H formation is indeed a precursor to this product (however, the HPLC response factor for CSO_3H is much lower than that for CSO_2H making CSO_3H difficult to detect at low concentrations).

As a more rigorous quantitative test, a mathematical model representing the reactions in Scheme I (Eqs. 3–7) was employed to fit each set of concentration *versus* time profiles shown in Fig. 3 along with the reactant concentrations (not shown). The solid lines in Fig. 3 reflect the best fits of this model and the parameters generated are listed in Table II. The model was clearly capable of fitting each group of the concentration *versus* time data separately and generating reasonable parameter values over the range of CSH:H_2O_2 ratios, which provides further support for the model. Transformed parameters representing the overall rate constant for disappearance of CSOH ($k_2 + k_3$) and the ratio of the rate constant for CSSC formation to the overall rate constant for CSOH disappearance $k_2/(k_2 + k_3)$ were employed in the place of k_2 and k_3 due to a significant correlation between k_2 and k_3. This provided excellent statistics for k_1, the rate constant for formation of reactive intermediate and for the fraction of the intermediate going to either product, but poor statistics for the sum of $k_2 + k_3$, as judged by the 95% confidence limits. It is reasonable that the 95% limits for $k_2 + k_3$ should be large, because k_1 reflects the rate-determining step. (Due to the paucity of data at pH 6, confidence limits could not be determined for $k_2 + k_3$ in some cases.)

Compared to the reaction in aqueous solution at pH 4.0 (28), the rate constant for the rate determining step, k_1, in amorphous PVP is $\sim 1–2\times10^5$-fold smaller. However, the values in Table II are based on lyophile concentrations of CSH and H_2O_2 which exceed the concentrations in the solutions from which the lyophiles were prepared by ~100-fold. Thus, the actual initial rate of reaction is ~10-fold slower in 'pH 4' lyophiles than in water at pH 4. In the amorphous state k_1 is nearly the same at pH 4 and pH 6 indicating that the overall reaction rate in this pH range is pH independent (and therefore evidently involving CSH rather than CS^- as the reactant), in stark contrast to the situation in aqueous solution where k_1 is first order in [OH^-], indicating that CS^- is the nucleophile in the first reaction step. As a result, the initial reaction rate is slower in 'pH 6' lyophiles than in water at pH 6. The reaction at 'pH 6' produces a modestly higher fraction of CSSC product, consistent with some contribution of CS^- in the second reaction step.

Although most features of the reaction in amorphous PVP are consistent with Scheme I, the mathematical model described in Eqs. (3)–(7) could not adequately fit all of the initial rate data in Table II simultaneously. An explanation for the ultimate failure of this simple model seems to reside in a small but systematic dependence of the rate constants on the [CSH]:[H_2O_2] composition. This is explored in greater detail in Figs. 7 and 8. In Fig. 5, log–log plots of the initial rates of total product formation *versus* the initial concentrations $[CSH]_0$ or $[H_2O_2]_0$ are shown for the reaction in aqueous solution and in amorphous PVP. In aqueous solution the formation of CSSC is first-order in $[CSH]_0$ and $[H_2O_2]_0$ and quantitatively consistent with Scheme I, while in amorphous PVP the apparent reaction order is 0.76 (0.72) with respect to [H_2O_2] and 1.27 (1.17) with respect to [CSH] at 'pH 4' ('pH 6'). This reduced sensitivity to $[H_2O_2]_0$ and heightened sensitivity to $[CSH]_0$ are also revealed in the systematic variation in both k_1 and $k_2/(k_2 + k_3)$ (and therefore $k_3/(k_2 + k_3)$) at 'pH 4' and also 'pH 6,' as shown in Fig. 6. At constant $[CSH]_0$, increasing $[H_2O_2]_0$ over an approximately six-fold range results in an ~37–47% reduction in k_1, thus reducing the slope in log ($d[CSSC]/dt + d[CSO_2H]/dt$) *versus* $[H_2O_2]_0$ to a value less than one. At

constant $[H_2O_2]_0$, increasing $[CSH]_0$ over an eight-fold range resulted in a near doubling of k_1, giving rise to a slope >1 in log (d[CSSC]/dt + d[CSO_2H]/dt) *versus* $[CSH]_0$. Parallel influences were seen in the effects of [CSH]:$[H_2O_2]$ composition on $k_3/(k_2 + k_3)$ (Fig. 6). While increasing $[H_2O_2]_0$ increases the fraction of CSO_2H degradant formed, the increase is less than the model in Eqs. 3–7 predicts due to a reduction in $k_3/(k_2 + k_3)$. In contrast, increasing $[CSH]_0$ produces a greater fraction of CSSC degradant, but less than that predicted by the model because $k_3/(k_2 + k_3)$ increases.

The systematic variation in rate constants with [CSH]:$[H_2O_2]$ composition may indicate that the distribution of these molecules is not uniform throughout the PVP matrix. Rather, spatial heterogeneity in their distribution may occur due to a preference of these solutes to localize in pockets of high water content or due to their potential to themselves form hydrogen bonded clusters. Previously, molecular dynamics simulations (24) demonstrated that the distribution of water in an amorphous PVP glass is highly heterogeneous at 10% w/w water (comparable to the water content in the lyophiles in the present study), reflecting the formation of water strands or small clusters occupying the channels between polymer chains rather than complete phase separation. These water clusters gave rise to an enhanced local mobility with increasing water content. Experimentally in PVP under ambient conditions, Lebedeva *et al.* (48) identified clusters consisting of four water molecules associated with two neighboring polymer units.

H_2O_2 forms stronger hydrogen bonds than water because it is a stronger acid (pK_a (H_2O_2) = 11.5 (28) *versus* 15.75 for water). Panarin *et al.* (49) confirmed that H_2O_2 molecules form stronger hydrogen bonds than water with the carbonyl oxygen atom in PVP and that strong self-association of H_2O_2 can occur in PVP, leading to extended ribbon structures of H_2O_2 complexed with PVP carbonyl oxygen atoms.

The reductions in rate constants observed in this study with increasing H_2O_2 ratios in PVP may reflect the formation of H_2O_2 clusters having reduced reactivity. Further studies will be needed to more thoroughly characterize these subtle composition effects.

Heterogeneous dynamics as manifested in non-mono-exponential decay kinetics are often seen in amorphous polymers (50–52) and frequently described by the empirical KWW equation (Eq. 9) (35–37). While this equation could also be applied to fit each of the concentration *versus* time curves generated in this study (Fig. 8), different parameter values were obtained (Table IV) depending on which species was monitored. This is understandable, given that the KWW equation cannot readily take into account the detailed chemistry and multiple reaction steps that are described in Scheme I.

An alternative approach for describing local motions in amorphous polymers assumes molecules residing in different spatial locations have different rate constants and geometries of motion, such that they can be treated as sub-ensembles of mobile and less mobile components (53–55). Bohmer *et al.* (56) demonstrated in various glass-forming materials that "non-exponential relaxation results from a superposition of dynamically distinguishable entities," consistent with the existence of spatial heterogeneity. The simplest model for heterogeneous reaction dynamics consistent with Scheme I that could be tested assumes two populations of reactants having different reactivities (i.e., i = 2 in Eqs. 3–7). This model has an advantage over the KWW equation in that it has a conceptual basis, it is reasonable in light of the likely heterogeneous distributions of water, H_2O_2, and possibly cysteine in amorphous PVP, and it can be used in conjunction with Scheme I to simultaneously fit both reactant disappearance and product formation, as demonstrated by the solid lines in Fig. 2. The parameter values generated (Table IV) indicate that the data in Fig. 2 can be described by two approximately equal reactant populations having reactivities that differ by more than an order of magnitude.

CONCLUSIONS

When reactive intermediates are involved, differences in degradant profiles and other characteristics (e.g., rate constants, apparent reaction order) in the amorphous-state may simply reflect altered rates for individual reaction steps due to glass-induced changes in relative reactant mobilities rather than a change in overall mechanism. Compared with the reaction in solution where a single degradant (CSSC) is produced, CSH reacts with H_2O_2 in amorphous PVP to generate CSSC, CSO_2H and CSO_3H. While simple bimolecular kinetics govern the solution reaction, initial rates in amorphous PVP suggested more complex kinetics (i.e., non-unity values for reaction order). These differences in degradants and apparent reaction orders in the solid-state could be rationalized by a model that assumes that the same reactive intermediate (CSOH) forms in the amorphous solid-state reaction as in solution, but partitions to multiple products in the solid-state due to the restricted mobility of CSH. Beyond the initial rate region, the kinetics in amorphous PVP could be described by the Kohlrausch-Williams-Watts (KWW) stretched-exponential equation or by assuming two populations of reactant molecules having quite different reactivities.

Future studies will focus on more rigorous tests of the kinetic models suggested by the data in the present study.

ACKNOWLEDGMENTS

This work was made possible by a grant from Pfizer Inc. The authors thank Dr. Paul Bummer for allowing use of his DSC and Mr. Henry Francis for assistance in powder X-ray diffractometry. The use of the powder X-ray diffractometry facility in the Kentucky Geological Survey (KGS) of the University of Kentucky is also gratefully acknowledged.

REFERENCES

1. M. J. Pikal, A. L. Lukes, and J. E. Lang. Thermal decomposition of amorphous β-lactam antibiotics. *J. Pharm. Sci.* **66**:1312–1316 (1977).
2. S. M. Lievonen, T. J. Laaksonen, and Y. H. Roos. Nonenzymatic browning in food models in the vicinity of the glass transition:

effects of fructose, glucose, and xylose as the reducing sugar. *J. Agric. Food Chem.* **50**:7034–7041 (2002).
3. S. P. Duddu and K. Weller. Importance of glass transition temperature in accelerated stability testing of amorphous solids: case study using a lyophilized aspirin formulation. *J. Pharm. Sci.* **85**:345–347 (1996).
4. K. A. Connors. *Chemical Kinetics. The Study of Reaction Rates in Solution*, VCH, New York, NY, 1990.
5. S. Yoshioka and V. J. Stella. *Stability of Drugs and Dosage Forms*, Kluwer, New York, NY, 2000.
6. B. C. Hancock and M. Parks. What is the true solubility advantage of amorphous pharmaceuticals? *Pharm. Res.* **17**:397–404 (2000).
7. A. A. Ambike, K. R. Mahadik, and A. Paradkar. Spray-dried amorphous solid dispersions of simvastatin, a low Tg drug: *in vitro* and *in vivo* evaluations. *Pharm. Res.* **22**:990–998 (2005).
8. J. E. Carpenter, M. J. Pikal, B. S. Chang, and T. W. Randolph. Rational design of stable lyophilized protein formulations: some practical advice. *Pharm. Res.* **14**:969–975 (1997).
9. J. F. Carpenter, K.-I. Izutsu, and T. W. Randolph. Freezing- and drying-induced perturbations of protein structure and mechanisms of protein protection by stabilizing additives. In L. Rey and J. C. May (eds.), *Drugs Pharm. Sci., 96 (Freeze-Drying/ Lyophilization of Pharmaceutical and Biological Products*, Marcel Dekker, New York, 1999, p 123.
10. F. Franks, R. H. M. Hatley, and S. F. Mathias. Materials science and the production of shelf-stable biologicals. *Pharm. Technol.* **March**:32–50 (1992).
11. C. Ahlneck and G. Zografi. The molecular basis of moisture effects on the physical and chemical stability of drugs in the solid state. *Int. J. Pharm.* **62**:87–95 (1990).
12. Y. Aso, S. Yoshioka, J. Zhang, and G. Zografi. Effect of water on the molecular mobility of sucrose and poly(vinylpyrrolidone) in a colyophilized formulation as measured by 13_C-NMR relaxation time. *Chem. Pharm. Bull.* **50**:822–826 (2002).
13. Y. Guo, S. R. Byrn, and G. Zografi. Physical characteristics and chemical degradation of amorphous quinapril hydrochloride. *J. Pharm. Sci.* **89**:128–143 (2000).
14. B. C. Hancock, S. L. Shamblin, and G. Zografi. Molecular mobility of amorphous pharmaceutical solids below their glass transition temperatures. *Pharm. Res.* **12**:799–806 (1995).
15. B. C. Hancock and G. Zografi. Characteristics and significance of the amorphous state in pharmaceutical systems. *J. Pharm. Sci.* **86**:1–12 (1997).
16. C. A. Oksanen and G. Zografi. Molecular mobility in mixtures of absorbed water and solid poly(vinylpyrrolidone). *Pharm. Res.* **10**:791–799 (1993).
17. E. Y. Shalaev and G. Zografi. How does residual water affect the solid-state degradation of drugs in the amorphous state? *J. Pharm. Sci.* **85**:1137–1141 (1996).
18. C. A. Angell. Formation of glasses from liquids and biopolymers. *Science* **267**:1924–1935 (1995).
19. T.-X. Xiang and B. D. Anderson. A molecular dynamics simulation of reactant mobility in an amorphous formulation of a peptide in poly(vinylpyrrolidone). *J. Pharm. Sci.* **93**:855–876 (2004).
20. Y. Gebremichael, T. B. Schroder, F. W. Starr, and S. C. Glotzer. Spatially correlated dynamics in a simulated glass-forming polymer melt: analysis of clustering phenomena. *Phys. Rev. E* **64**:051503-1-13 (2001).
21. W. Jin and R. H. Boyd. Time evolution of dynamic heterogeneity in a polymeric glass: A molecular dynamics simulation study. *Polymer* **43**:503–507 (2002).
22. S. A. Hill, W. MacNaughtan, I. A. Farhat, T. R. Noel, R. Parker, S. G. Ring, and M. J. Whitcomb. The effect of thermal history on the Maillard reaction in a glassy matrix. *J. Agric. Food Chem.* **53**:10213–10218 (2005).
23. T. W. Randolph. Phase separation of excipients during lyophilization: effects on protein stability. *J. Pharm. Sci.* **86**:1198–1203 (1997).
24. T.-X. Xiang and B. D. Anderson. Distribution and effect of water content on molecular mobility in poly(vinylpyrrolidone) glasses: a molecular dynamics simulation. *Pharm. Res.* **22**:1205–1214 (2005).
25. P.-S. K. Leung and M. R. Hoffmann. Kinetics and mechanism of the oxidation of 2-mercaptoethanol by hydrogen peroxide in aqueous solution. *J. Phys. Chem.* **89**:5267–5271 (1985).
26. C. C. Winterbourn and D. Metodewa. Reactivity of biologically important thiol compounds with superoxide and hydrogen peroxide. *Free Radic. Biol. Med.* **27**:322–328 (1999).
27. J. P. Barton, J. E. Packer, and R. J. Sims. Kinetics of the reaction of hydrogen peroxide with cysteine and cysteamine. *J. Chem. Soc., Perkin Trans. II* **1973**:1547–1549 (1973).
28. D. Luo, S. W. Smith, and B. D. Anderson. Kinetics and mechanism of the reaction of cysteine and hydrogen peroxide in aqueous solution. *J. Pharm. Sci.* **94**:304–316 (2005).
29. Y. H. Zhao, M. H. Abraham, and A. M. Zissimos. Determination of McGowan volumes for ions and correlation with van der Waals volumes. *J. Chem. Inf. Comput. Sci.* **43**:1848–1854 (2003).
30. C. W. Jones. *Applications of Hydrogen Peroxide and Derivatives*, Royal Society of Chemistry, Cambridge, UK, 1999.
31. B. S. Chang and C. S. Randall. Use of subambient thermal analysis to optimize protein lyophilization. *Cryobiology* **29**: 632–656 (1992).
32. L. S. Taylor, F. W. Langkilde, and G. Zografi. Fourier transform raman spectroscopic study of the interaction of water vapor with amorphous polymers. *J. Pharm. Sci.* **90**:888–901 (2001).
33. T. Huang, M. E. Garceau, and P. Gao. Liquid chromatographic determination of residual hydrogen peroxide in pharmaceutical excipients using platinum and wired enzyme electrodes. *J. Pharm. Biomed. Anal.* **31**:1203–1210 (2003).
34. C. Vignaud, L. Rakotozafy, A. Falguieres, J. Potus, and J. Nicolas. Separation and identification by gel filtration and high-performance liquid chromatography with UV or electrochemical detection of the disulphides produced from cysteine and glutathione oxidation. *J. Chromatog. A* **1031**:125–133 (2004).
35. R. Kohlrausch. Theorie des electrischen Rückstandes in der Leidner Flasche. *Pogg. Ann. Phys. Chem.* **91**:179–214 (1854).
36. G. Williams and D. C. Watts. Non-symmetrical dielectric relaxation behavior arising from a simple empirical decay function. *Trans. Faraday Soc.* **66**:80–85 (1970).
37. G. Williams, D. C. Watts, S. B. Dev, and A. M. North. Further considerations of non symmetrical dielectric relaxation behaviour arising from a simple empirical decay function. *Trans. Faraday Soc.* **67**:1323–1335 (1971).
38. T. Geiger and S. Clarke. Deamidation, isomerization, and racemization at asparaginyl and aspartyl residues in peptides. Succinimide-linked reactions that contribute to protein degradation. *J. Biol. Chem.* **262**:785–794 (1987).
39. R. T. Darrington and B. D. Anderson. Evidence for a common intermediate in insulin deamidation and covalent dimer formation: effects of pH and aniline trapping in dilute acidic solutions. *J. Pharm. Sci.* **84**:275–282 (1995).
40. R. G. Strickley and B. D. Anderson. Solid-state stability of human insulin I. Mechanism and the effect of water on the kinetics of degradation in lyophiles from pH 2-5 solutions. *Pharm. Res.* **13**:1142–1153 (1996).
41. R. G. Strickley and B. D. Anderson. Solid-state stability of human insulin. II. Effect of water on reactive intermediate partitioning in lyophiles from pH 2–5 solutions - stabilization against covalent dimer formation. *J. Pharm. Sci.* **86**:645–653 (1997).
42. H. R. Costantino, R. Langer, and A. M. Klibanov. Aggregation of a lyophilized pharmaceutical protein, recombinant human albumin: effect of moisture and stabilization by excipients. *Biotechnology* **13**:493–496 (1995).
43. D. B. Volkin and A. M. Klibanov. Thermal destruction processes in proteins involving cystine residues. *J. Biol. Chem.* **262**:2945–2950 (1987).
44. S. E. Zale and A. M. Klibanov. Why does ribonuclease irreversibly inactivate at high temperatures?. *Biochem.* **25**: 5432–5444 (1986).
45. Z. Qiu, J. G. Stowell, K. R. Morris, S. R. Byrn, and R. Pinal. Kinetic study of the Maillard reaction between metoclopramide hydrochloride and lactose. *Int. J. Pharm.* **303**:20–30 (2005).
46. S. W. Griffiths, J. King, and C. L. Cooney. The reactivity and oxidation pathway of cysteine 232 in recombinant human α1-antitrypsin. *J. Biol. Chem.* **277**:25486–25492 (2002).

47. F. Fujara, B. Geil, H. Sillescu, and G. Fleischer. Translational and rotational diffusion in supercooled orthoterphenyl close to the glass transition. *Z. Phys. B: Condens. Matter* **88**:195–204 (1992).
48. T. L. Lebedeva, S. A. Kuptsov, M. M. Feldstein and N. A. Plate. Molecular arrangement of water associated with poly(N-vinyl pyrrolidone) in the first hydrate shell. In A. L. Iordanskii, O. V. Startsev, and G. E. Zaikov (eds.), *Water Transport in Synthetic Polymers*, Topchiev Institute of Petrochemical Synthesis, Russian Academy of Sciences, Moscow, Russia, 2003, pp. 69–93.
49. E. F. Panarin, K. K. Kalninsh, and D. V. Pestov. Complexation of hydrogen peroxide with polyvinylpyrrolidone: *ab initio* calculations. *Eur. Polym. J.* **37**:375–379 (2001).
50. R. Richert. Heterogeneous dynamics in liquids: fluctuations in space and time. *J. Phys.: Condens. Matter* **14**:R703–R738 (2002).
51. M. Levitus, M. Talhavini, R. M. Negri, T. D. Z. Atvars, and P. F. Aramendia. Novel kinetic model in amorphous polymers. Spiropyran-merocyanine system revisited. *J. Phys. Chem. B.* **101**:7680–7686 (1997).
52. J.-W. Park, M. D. Ediger, and M. M. Green. Chiral studies in amorphous solids: the effect of the polymeric glassy state on the racemization kinetics of bridged paddled binaphthyls. *J. Am. Chem. Soc.* **123**:49–56 (2001).
53. K.-L. Li, A. A. Jones, P. T. Inglefield, and A. D. English. Domain size of dynamic heterogeneities just above the glass transition in an amorphous polycarbonate. *Macromolecules* **22**:4198–4204 (1989).
54. S. C. Glotzer. Spatially heterogeneous dynamics in liquids: insights from simulation. *J. Non-Cryst. Solids* **274**:342–355 (2000).
55. M. D. Ediger. Spatially heterogeneous dynamics in supercooled liquids. *Annu. Rev. Phys. Chem.* **51**:99–128 (2000).
56. R. Bohmer, R. V. Chamberlin, G. Diezemann, B. Geil, A. Heuer, G. Hinze, S. C. Kuebler, R. Richert, B. Schiener, H. Sillescu, H. W. Spiess, U. Tracht, and M. Wilhelm. Section 1. Dynamic heterogeneity nature of the non-exponential primary relaxation in structural glass-formers probed by dynamically selective experiments. *J. Non-Cryst. Solids* **235**–**237**:1–9 (1998).